CLM - P 204

United Kingdom Atomic Energy Authority
RESEARCH GROUP

Preprint

ATTENUATION OF AN ELECTROMAGNETIC WAVE IN A LOW DENSITY CYLINDRICAL PLASMA

H. BLEVIN
J. A. REYNOLDS
P. C. THONEMANN

Culham Laboratory
Abingdon Berkshire

1969

UNCLASSIFIED
Approved for Publication

CLM - P 204

ATTENUATION OF AN ELECTROMAGNETIC WAVE IN A LOW DENSITY CYLINDRICAL PLASMA

by

H. Blevin
J.A. Reynolds
P.C. Thonemann

A B S T R A C T

Measurements of the attenuation of an electromagnetic wave in a cylindrical plasma of electron density between 10^{10} and nearly 10^{11} cm^{-3}, electron temperature 2·2 eV and electron collision frequency for momentum transfer 1·2 MHz agree with an elementary theory using the Lorentz conductivity. Small deviations observed for an electron density of 10^{11} cm^{-3} and a wave frequency of a few MHz are ascribed to the appreciable electron thermal velocity. The electron density and collision frequency deduced from the attenuation agree with Langmuir probe measurements. The influence of the magnetic probe size, density gradients and finite Debye length are shown to be small.

U.K.A.E.A. Research Group,
Culham Laboratory,
Abingdon,
Berks.

February, 1969 (SLW)

CONTENTS

1. INTRODUCTION

Interest in the attenuation of electromagnetic waves in plasma arises because of their importance in heating, communications and high frequency containment. Elementary theory relates the attenuation to the Lorentz conductivity $\sigma = ne^2/m(\nu - i\omega)$ where ω is the wave angular frequency and n, e, m and ν are the electron density, charge, mass and collision rate for momentum transfer respectively. However, when the electron temperature and mean free path are appreciable the conductivity must be modified to allow for the non-local relationship between the current density and electric field, producing effects similar to the anomalous skin depth observed in metals[1,2]. Weibel's[3] calculations for a semi-infinite plane plasma show that the attenuation is then not exponential or, in general, monotonic because electrons carry momentum acquired near the plasma surface to deeper layers where they are out of phase with the field. Experimentally, these effects are usually further complicated by cylindrical geometry which introduces the plasma radius and further boundary conditions.

The object of this investigation was to determine experimentally the range of applicability of the elementary theory using a cylindrical plasma. The procedure was to compare the elementary theory to the ratio of the amplitude of the magnetic field at the plasma surface to the amplitude of the magnetic field at the plasma axis measured as a function of wave frequency for various fixed electron densities. The wave frequency was between $0{\cdot}1\ \nu$ and $10\ \nu$ and the electron density between 10^{10} and 10^{11} cm^{-3}. Over the greater part of the frequency and electron density ranges the elementary theory applied, provided suitable values of electron density and collision rate were chosen.

These values were close to those measured by Langmuir probes. Significant deviations from the elementary theory were only found for the highest electron density and wave frequencies a few times the collision frequency. These appeared as an enhanced screening rather than an enhanced penetration.

Previous investigations[4-7] have been carried out in plasmas maintained by the wave itself thus leading to doubts about the constancy of the electron temperature and density, an electron cyclotron frequency much greater than the wave frequency, and a cyclotron radius comparable or small compared to the measured skin depth. In the present work a small amplitude wave penetrated the positive column of a low pressure mercury arc maintained by a steady axial current. The electron cyclotron radius in both the wave magnetic field and the magnetic field of the axial current was greater than the plasma radius, and the wave contributed a negligible energy to the plasma.

The wave attenuation is calculated on the elementary theory by combining Maxwell's equations (using electromagnetic units)

$$\nabla \times \underline{B} = 4\pi \underline{J} - \frac{i\omega}{c^2} \underline{E} \quad \text{and} \quad \nabla \times \underline{E} = i\omega \underline{B} \qquad \ldots (1)$$

with the Lorentz conductivity[8]

$$\sigma = \frac{J}{E} = \frac{ne^2}{m} \left(\frac{1}{\nu - i\omega} \right) \qquad \ldots (2)$$

where $\underline{B}$ and $\underline{E}$ are the wave electric and magnetic fields (taken as proportional to $\exp(-i\omega t)$ and J is the current density. It is assumed that the velocity distribution is isotropic but not necessarily Maxwellian, the perturbation produced by the wave is small, and the electron collision rate for momentum transfer is independent of electron velocity (see Figure 7). In cylindrical coordinates, taking

B parallel to the axis, equations (1) and (2) give

$$\frac{1}{rB}\frac{\partial}{\partial r}\left(r\frac{\partial B}{\partial r}\right) = \frac{1}{\delta^2}\left(\frac{\omega}{\omega + i\nu}\right) - \frac{\omega^2}{c^2} \qquad \ldots (3)$$

where δ is the collisionless skin depth = $(mc^2/4\pi ne^2)^{\frac{1}{2}}$.

In these experiments the wave frequency was much less than the plasma frequency (c/δ) so we may neglect the displacement current term ω^2/c^2. The boundary conditions that the magnetic field at the plasma surface (radius a) is B_a, and the magnetic field on the axis (zero radius) is B_o, then give the solution of equation (3)

$$\frac{B_a}{B_o} = I_o\left(\frac{a}{\delta}\sqrt{\frac{\omega}{\omega + i\nu}}\right) \qquad \ldots (4)$$

This is the basic equation which we compare to our experimental results. To use it we separate the real and imaginary parts by expanding the Bessel function according to[9]

$$I_o(x) = \sum_{N=0}^{\infty} \frac{\left(\frac{x}{2}\right)^{2N}}{(N!)^2} \qquad \ldots (5)$$

so that B_a/B_o may be expressed in the form

$$\frac{B_a}{B_o} = A\, e^{i\theta} \qquad \ldots (6)$$

where A is the ratio of the amplitude of the magnetic field at the plasma surface to the magnetic field at the axis and θ is the phase difference between the surface and axial magnetic field. For the particular experimental parameters investigated the maximum value of A was about 3, and an accuracy to within 1% is obtained by using the first four terms of the Bessel expansion.

For very high frequencies, when $\omega \gg \nu$, equation (4) tends to the limit

$$\frac{B_a}{B_o} = I_o\left(\frac{a}{\delta}\right) \qquad \ldots (7)$$

and the ratio of the magnetic field at the plasma surface to the magnetic field on the axis is independent of frequency and depends only on the ratio of the plasma radius to collision free skin depth. Also, since B_a/B_o is real there is no phase difference.

On the other hand, at very low frequencies we may expand equation (4) as a series in ω/ν:

$$I_o\left(\frac{a}{\delta}\sqrt{\frac{\omega}{\omega + i\nu}}\right) = 1 - i\left(\frac{a}{2\delta}\right)^2\left(\frac{\omega}{\nu}\right) + \left(\frac{a}{2\delta}\right)^2\left[1 - \left(\frac{1}{2!}\right)^2\left(\frac{a}{2\delta}\right)^2\right]\left(\frac{\omega}{\nu}\right)^2 + \ldots$$

It should be noted that only when $a/\delta \gg 4$ this becomes

$$I_o\left(\frac{a}{\delta}\sqrt{\frac{\omega}{i\nu}}\right) = 1 - i\left(\frac{a}{2\delta}\right)^2\left(\frac{\omega}{\nu}\right) - \left(\frac{1}{2!}\right)^2\left(\frac{a}{2\delta}\right)^4\left(\frac{\omega}{\nu}\right)^2 + \ldots$$

$$= \mathrm{ber}_o\left(\frac{a\sqrt{2}}{\delta_c}\right) - i\,\mathrm{bei}_o\left(\frac{a\sqrt{2}}{\delta_c}\right)$$

where δ_c = collisional skin depth = $\delta\sqrt{\frac{2\nu}{\omega}}$. As $\omega \to 0$, the imaginary part of $I_o\left(\frac{a}{\delta}\sqrt{\frac{\omega}{\omega + i\nu}}\right) \to 0$ and so the phase difference tends to zero. A semi-log plot of the phase difference against wave frequency is almost symmetrical about a peak near $\omega = \nu$ (see Figure 3) where, for $a/\delta \ll 2$

$$\tan\theta = \frac{1}{8}\left(\frac{a}{\delta}\right)^2 \qquad \ldots (8)$$

2. APPARATUS

The positive column of a mercury arc maintained by a steady current was chosen since it has been studied for many years and is well understood[10].

A diagram of the apparatus is shown in Figure 1. The typical operating conditions are shown in Table I.

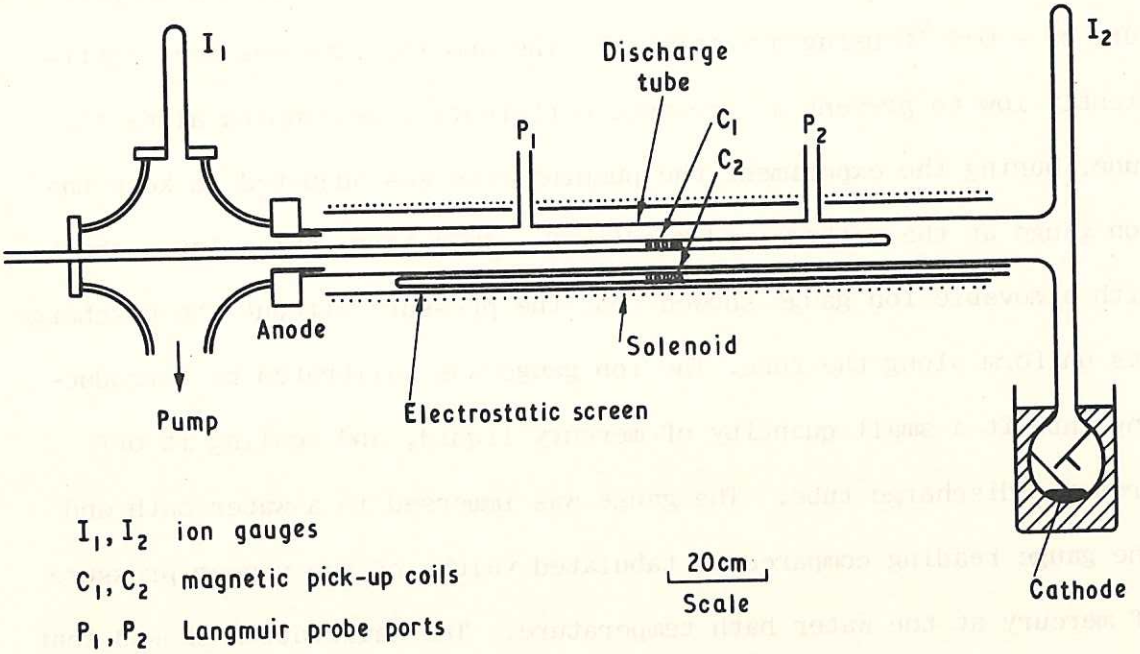

Fig. 1 Apparatus (CLM-P 204)

Neutral density	$1{\cdot}0 \times 10^{13}$ cm^{-3}
Electron density	10^{10} to 10^{11} cm^{-3} (according to arc current)
Electron temperature	about 2·2 eV
Electron collision frequency for momentum transfer	about 1·2 MHz
Arc current	0 to 17 amps
Anode-cathode potential difference	about 50 volts
Axial electric field in positive column	about 0·1 volts/cm

Table I. Typical operating conditions.

The plasma was contained in a glass tube 150 cm long and 8·1 cm internal diamter. A water cooled ring anode and a mercury pool cathode with a starter electrode and spray screen were used. The neutral atom pressure was controlled by keeping the cathode at a constant temperature of + 0·4 ^{o}C using a water bath. The pumping rate was kept sufficiently low to prevent a pressure differential developing along the tube. During the experiment the pumping rate was adjusted to keep the ion gauge at the cathode end reading 8×10^{-4} torr, and a later check with a movable ion gauge showed that the pressure without the discharge was uniform along the tube. The ion gauge was calibrated by introducing into it a small quantity of mercury liquid, and sealing it off from the discharge tube. The gauge was immersed in a water bath and the gauge reading compared to tabulated values of the vapour pressure of mercury at the water bath temperature. The calibration showed that the neutral atom density was $1{\cdot}0 \times 10^{13} cm^{-3}$.

The electromagnetic field was generated by a 15 cm diameter 80 cm long solenoid placed coaxially with the plasma cylinder so that the induced electric field was circumferential, the magnetic field axial and the propagation radial. Standing waves and self resonances in the coil were avoided up to 13 MHz frequency by making the solenoid of 8 equal sections each shorter than the diameter. These sections were 10 cm long with 5 turns and were connected in parallel to the 195 Ω output of a distributed amplifier fed by a wide range oscillator. The coil was electrostatically screened from the plasma by 7·5 cm wide plastic strips in which many parallel 1 mm wide copper strips were embedded 1 mm apart (commercially known as "Biccastrip"). These were placed under the tube coil with the copper strips parallel to the axis, connected together at one end and earthed. The large ratio of length to diameter of both the coil and plasma reduced end effects.

The amplitude of the wave electric field at the plasma surface was less than 10^{-3} volts/cm. Since this was only 1% of the axial electric field in the plasma, the resulting perturbation of the electron velocity distribution was insufficient to change the average electron density and energy.

The wave magnetic field was detected by two identical coils, one placed on the plasma axis and the other placed outside the discharge tube. Each consisted of 50 turns wound on a 0·6 cm diameter former and screened by a slotted brass tube. The capacity between the coil and screen was sufficiently small to keep self resonances above 13 MHz. The signal was detected on either an oscilloscope or a milli-voltmeter. The two coils were cross-calibrated for relative sensitivity without the plasma, then the relative signals with the plasma present were measured and the attenuation calculated. The frequency range covered was 0·1 to 13 MHz.

The phase difference between the magnetic field at the plasma surface and the magnetic field at the plasma axis was measured as a function of frequency by triggering the oscilloscope at a constant time in the cycle using the signal from the coil external to the plasma, and observing the change in phase when the axial probe was moved to the plasma edge (the tube which contained the probe was supported on a system that could swing it from side to side of the discharge tube). The signal from the probe in the plasma was sinusoidal with no visual distortion, so the change in time at which the signal was zero gave the phase change. Triggering jitter produced a reading limit of ± 0·1 cm on a 0·02 μsec/cm time base, which is equivalent to ± 3·6 degrees at 5 MHz wave frequency.

3. MAGNETIC FIELD RATIO AND PHASE MEASUREMENTS

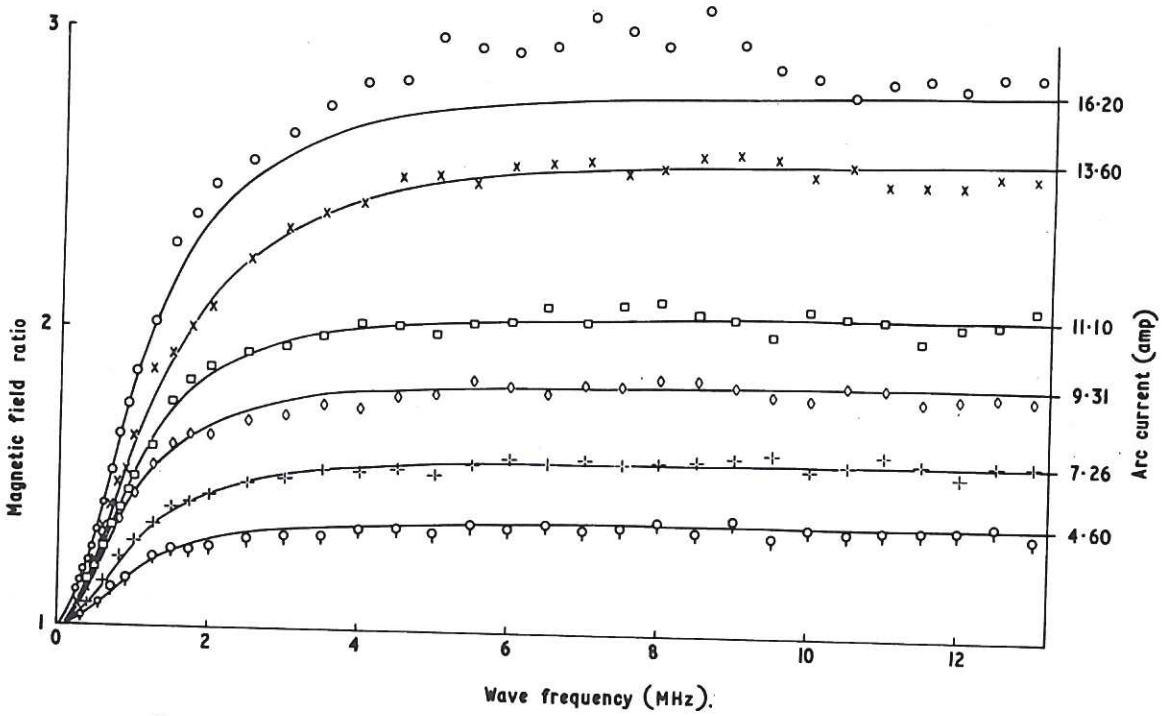

Fig. 2
Magnetic field ratio as a function of frequency for various arc currents compared to equation (4) using the parameters given in Table II

(CLM-P 204)

Figure 2 shows the ratio of magnetic field at the plasma surface to the magnetic field at the plasma axis measured as a function of frequency from 0·1 to 13 MHz for fixed arc currents (which are proportional to the electron density). The field ratio rises with increasing frequency tending to a constant value above a few MHz. This is interpreted as collisional attenuation below $\omega \sim \nu$ changing to collisionless attenuation well above $\omega \sim \nu$. Each curve in figure 2 is plotted from equation 4 chosing the constant parameters n and ν (given in table II) to give the best fit with the measurements over the whole frequency range. It can be seen that the agreement is good except for the highest electron density where it was not possible to get a good fit at all frequencies for a single value of electron density. Preliminary measurements using higher arc currents and an

extended frequency range showed that the majority of the descrepancy was an enhanced field ratio in the region of a few MHz, rather than a reduced field ratio at higher frequencies.

Arc current (amps)	Collision frequency ($\nu/2\pi$ sec^{-1})	Electron density (cm^{-3})
16·2	$1{\cdot}11 \cdot 10^{6}$	$9{\cdot}11 \cdot 10^{10}$
13·6	$1{\cdot}29 \cdot 10^{6}$	$8{\cdot}24 \cdot 10^{10}$
11·1	$1{\cdot}00 \cdot 10^{6}$	$5{\cdot}99 \cdot 10^{10}$
9·31	$0{\cdot}96 \cdot 10^{6}$	$4{\cdot}87 \cdot 10^{10}$
7·26	$1{\cdot}09 \cdot 10^{6}$	$3{\cdot}54 \cdot 10^{10}$
4·60	$1{\cdot}04 \cdot 10^{6}$	$2{\cdot}36 \cdot 10^{10}$

Table II. Parameters used in equation (4) to fit the experimental results of Figure 2.

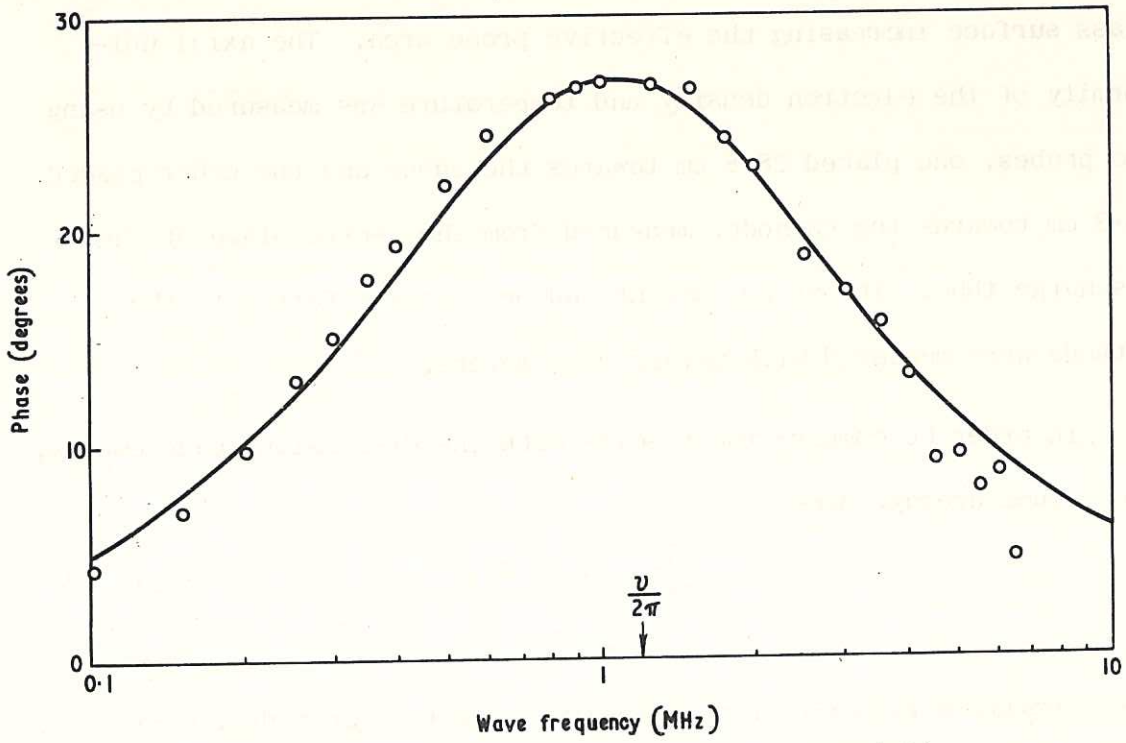

Fig. 3 (CLM-P 204)
Phase difference between the wave at the plasma surface and the wave at the plasma axis as a function of frequency for an arc current of 13.6 amps. (Electron density 8.24×10^{10} cm^{-3})

Figure 3 shows the measured phase difference between the magnetic field at the plasma surface and the magnetic field at the plasma axis as a function of frequency for an arc current of 13·6 amps. The points are close to a curve plotted from equation (4) using the same parameters as were used to fit equation (4) to the measured magnetic field ratio shown in figure 2 (electron density $8{\cdot}24 \cdot 10^{10}$ cm^{-3} and collision frequency $1{\cdot}29 \cdot 10^{6}$ sec^{-1}). The measured phase peaks near $\omega = \nu$ and tends to zero for $\omega \ll \nu$ and $\omega \gg \nu$, as predicted for collisional and collisionless conditions respectively.

4. MEASUREMENT OF THE ELECTRON DENSITIES AND COLLISION FREQUENCIES USING A LANGMUIR PROBE

Current was drawn from the plasma to the end of a 0·3 cm diameter tungsten wire probe which was ground flat and flush with the end of a supporting glass tube. A small gap of 0·005 cm between the inside of the glass tube and the probe prevented conduction currents on the glass surface increasing the effective probe area. The axial uniformity of the electron density and temperature was measured by using two probes, one placed 28·8 cm towards the anode and the other placed 28·8 cm towards the cathode, measured from the centre plane of the discharge tube. The probe current and potential referred to the cathode were measured with moving coil meters.

In order to compare the results with the dispersion measurements, the volume average density,

$$\bar{n} = \frac{1}{\pi a^2} \int_0^a 2\pi \, rn \, dr \qquad \ldots (9)$$

was calculated rather than the density at particular radial positions. The measurement was made by placing the probe at the discharge tube wall, and measuring the flux of positive ions moving to the wall under

the action of the radial electric field of the sheath. Since there was no probe immersed in the plasma, the effect of the probe on the plasma potential and electron density is to a great extent avoided. Langmuir's[10] theory of a plasma arc may be used to calculate the average electron density from the ion current to the wall.

For an arc with rate of ionization proportional to the electron density and an ion mean free path greater than the radius, the ion current density is given by

$$I = \frac{e}{2\pi a} \int_0^a n\, n_o \langle \sigma v \rangle 2\pi r\, dr \qquad \ldots (10)$$

where n_o is the neutral density and $\langle \sigma v \rangle$ is the ionization cross section times the electron velocity averaged over the electron velocity distribution. Since the ionization level was small and experimentally we observed the electron temperature to be uniform, the ionization rate per electron $n_o \langle \sigma v \rangle$ was independent of radius. Combining equations (9) and (10)

$$I = e \frac{a}{2} n_o \langle \sigma v \rangle \bar{n} \qquad \ldots (11)$$

Langmuir[10] has shown that, if we assume that at all points in the plasma the ion density is equal to the electron density, the plasma potential is related to the radius by

$$\frac{1}{s} \int_0^s \frac{s_z ds_z e^{-\eta_z}}{\sqrt{\eta - \eta_z}} - e^{-\eta} = 0 \qquad \ldots (12)$$

where η is the dimensionless potential $-\frac{eV}{kT}$ (V is the potential referred to the axis, T is the electron temperature and k is Boltzmann's constant), s is the dimensionless radius $r\, n_o \langle \sigma v \rangle \sqrt{\frac{M}{2kT}}$ (M is the ion mass), and the subscript z refers to a variable

radius z. Very near the wall the assumption that the ion density is the same as the electron density breaks down and the solution of equation (12) gives

$$s_a^1 = 0{\cdot}7722 = a\, n_o \langle \sigma v \rangle \sqrt{\frac{M}{2kT}} \qquad \ldots (13)$$

With equation (11), these numbers give the ion current density to the wall

$$I = 0{\cdot}546\, \bar{n}\, e \sqrt{\frac{kT}{M}} \qquad \ldots (14)$$

This equation is almost the same as the Bohm[11] equation except for a slight change in the numerical constant from 0·566 to 0·546, and here we specifically define the density obtained as the volume average density. Experimentally the ion current density to the wall was measured by plotting the current to a probe placed at the wall as a function of potential with respect to the cathode. In order to obtain reproducible readings, the probe was heated (by applying a large positive potential) for a few minutes; it is probable that this removed surface layers of impurities that accumulated when the discharge was not in operation. The probe potential included a small correction for the potential drop across the ammeter. Figures 4 and 5 show typical probe current/potential plots. The electron density is calculated from the ion current given in Figure 4 and the electron temperature from the slope of Figure 5.

The graph for negative probe currents should, for an ideal probe, saturate as the potential is decreased since all electrons are repelled and the current is wholly the positive ion flux leaving the plasma under the influence of the space charge electric field. In fact, the graph shows a gradual increase in current with increasingly negative probe potentials, possibly because the highly negative probe changes

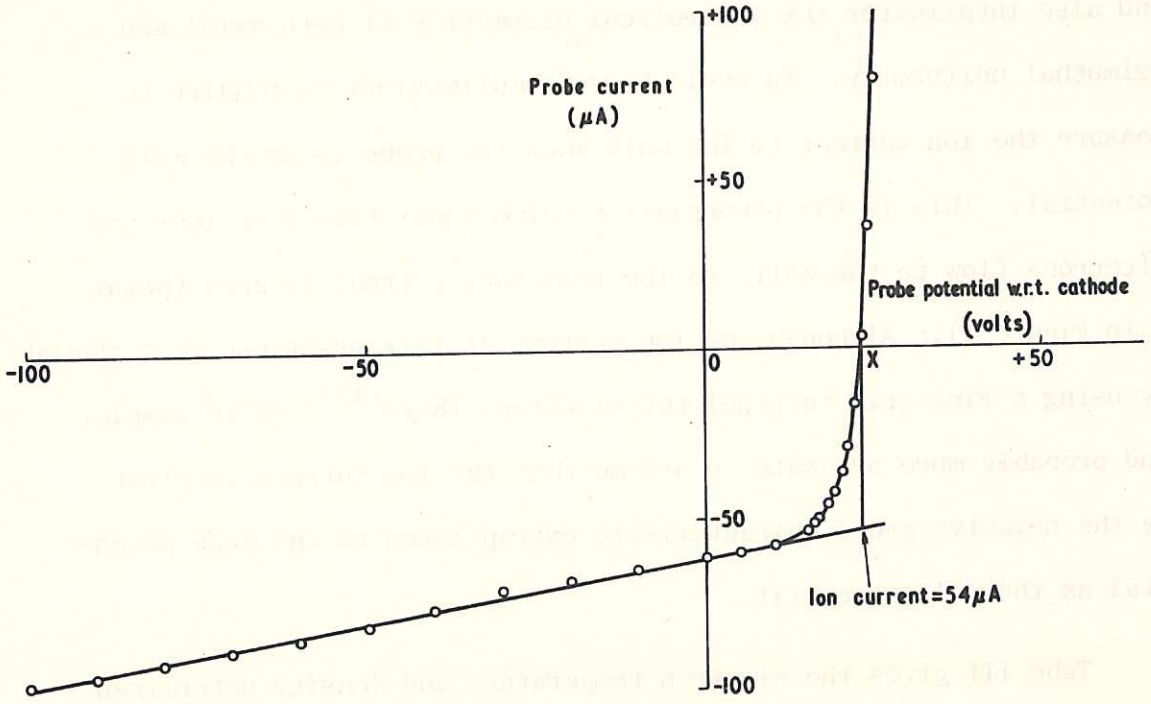

Fig. 4 (CLM-P 204)
Negative probe plot for an arc current of 13.6 amps

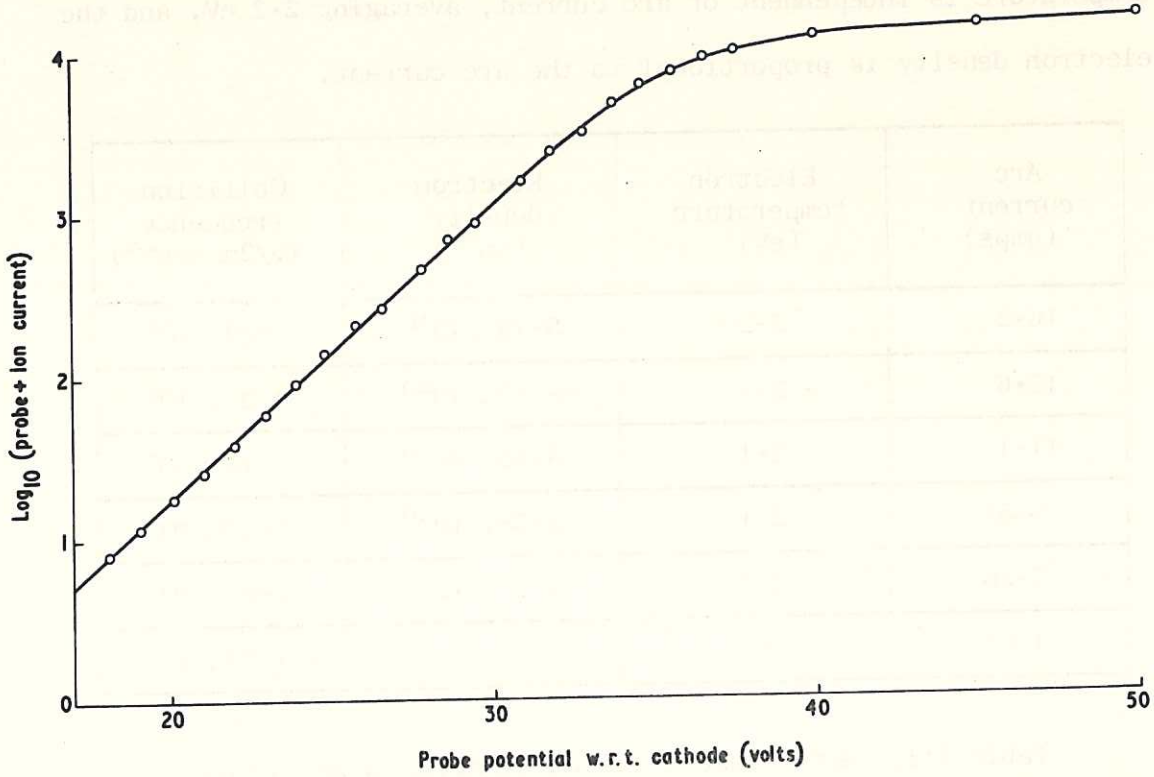

Fig. 5 (CLM-P 204)
Positive probe plot for an arc current of 13.6 amps.

the plasma potential distribution which affects the sheath thickness and also invalidates the theoretical assumption of both axial and azimuthal uniformity. To avoid these complications we require to measure the ion current to the wall when the probe is at the wall potential. This is the potential at which equal fluxes of ions and electrons flow to the wall, so the resultant current is zero (point x in Figure 4). Although the ion current at this point can be measured by using a fine grid to repel the electrons (Boyd[12]) it is simpler and probably more accurate to assume that the ion current is given by the negative probe characteristic extrapolated to the same potential as the wall potential.

Tabe III gives the electron temperature and density determined from the Langmuir probe results for each of the arc currents used in the magnetic field ratio measurements given in figure 2. The electron temperature is independent of arc current, averaging 2·2 eV, and the electron density is proportional to the arc current.

Arc current (amps)	Electron temperature (eV)	Electron density (cm^{-3})	Collision frequency ($\nu/2\pi$ sec^{-1})
16·2	2·2	$9·76 \cdot 10^{10}$	$1·29 \cdot 10^{6}$
13·6	2·4	$8·10 \cdot 10^{10}$	$1·27 \cdot 10^{6}$
11·1	2·1	$6·45 \cdot 10^{10}$	$1·10 \cdot 10^{6}$
9·31	2·1	$5·38 \cdot 10^{10}$	$1·22 \cdot 10^{6}$
7·26	2·1	$3·75 \cdot 10^{10}$	$1·09 \cdot 10^{6}$
4·60	2·3	$2·75 \cdot 10^{10}$	$1·24 \cdot 10^{6}$

Table III. Arc Parameters from Langmuir probe results

Table III also gives the electron collision frequency $(\nu/2\pi)$ calculated from the potential drop (φ) down the plasma column accompanying the direct arc current. The potential drop was measured from the turn-over point to the electron saturation current for two Langmuir probes a distance $\ell = 57{\cdot}6$ cm apart. By equation (2) the d.c. conductivity is

$$\sigma = \frac{ne^2}{m\nu} = \frac{\ell J}{\varphi}$$

where J is the current density at a radius r. Using equation (9) we get

$$\nu = \frac{\pi(a^2 - b^2)e^2}{m\ell} \cdot \frac{\bar{n}\varphi}{I}$$

where I is the total arc current, $\pi(a^2 - b^2)$ is the cross sectional area of the arc, and $\bar{n}$ is the average electron density as measured by the Langmuir probe. The results show that the collision frequency is independent of the electron density, and has an average value of 1·2 MHz.

5. COMPARISON OF THE AVERAGE ELECTRON DENSITY AND COLLISION FREQUENCY REQUIRED TO FIT EQUATION (4) TO THE WAVE ATTENUATION MEASUREMENTS, TO VALUES FOUND USING LANGMUIR PROBES

Before comparing the electron densities, small corrections were made for the finite size of the magnetic probe and the electron density non-uniformity on the attenuation results, and the presence of the magnetic probe at the plasma axis and the finite Debye length on the Langmuir probe results. The calculations, which are in terms of the volume average electron density, are given in the Appendices, and the results are summarised in Table IV. This shows that in no case was the correction more than 4%.

Arc current (amps)	Wave attentuation corrections (%)		Langmuir probe corrections (%)	
	finite magnetic probe size	electron density non-uniformity	presence of magnetic probe	finite Debye length
16.2	+ 3•7	- 1•9	+ 1•3	- 1•4
13•6	+ 3•6	- 1•8	+ 1•3	- 1•7
11•1	+ 3•3	- 1•3	+ 1•3	- 1•7
9•31	+ 3•1	- 1•1	+ 1•3	- 1•8
7•26	+ 2•9	- 0•9	+ 1•3	- 2•2
4•60	+ 2•7	- 0•6	+ 1•3	- 2•7

Table IV. Corrections to the electron density measurements (see Appendices)

Arc current (amps)	Corrected electron density (cm^{-3})		Collision frequency (sec^{-1})	
	From Wave Attenuation	From Langmuir Probes	From Wave Attenuation	From Langmuir probes
16·2	$9{\cdot}3 \times 10^{10}$	$9{\cdot}8 \times 10^{10}$	$1{\cdot}1 \times 10^{6}$	$1{\cdot}3 \times 10^{6}$
13·6	$8{\cdot}4 \times 10^{10}$	$8{\cdot}1 \times 10^{10}$	$1{\cdot}3 \times 10^{6}$	$1{\cdot}3 \times 10^{6}$
11·1	$6{\cdot}1 \times 10^{10}$	$6{\cdot}4 \times 10^{10}$	$1{\cdot}0 \times 10^{6}$	$1{\cdot}1 \times 10^{6}$
9·31	$5{\cdot}0 \times 10^{10}$	$5{\cdot}4 \times 10^{10}$	$1{\cdot}0 \times 10^{6}$	$1{\cdot}2 \times 10^{6}$
7·26	$3{\cdot}6 \times 10^{10}$	$3{\cdot}7 \times 10^{10}$	$1{\cdot}1 \times 10^{6}$	$1{\cdot}1 \times 10^{6}$
4·60	$2{\cdot}4 \times 10^{10}$	$2{\cdot}7 \times 10^{10}$	$1{\cdot}0 \times 10^{6}$	$1{\cdot}2 \times 10^{6}$

Table V. Comparison of the average electron density and collision frequency required to fit equation (4) to the wave attenuation measurements to values found using Langmuir probes.

Table V compares the corrected average electron density and collision frequency required to fit equation (4) to the measured magnetic field ratios to the Langmuir probe results. The agreement shows that, within experimental error, the elementary theory expressed by equation (4) is applicable over most of the density range.

The result given in Table V may be expressed as a graph of collisionless skin depth measured from the wave attenuation plotted against the inverse of the square root of the average electron density measured by the Langmuir probe. This should be linear, through the origin and have a slope $(mc^2/4\pi e^2)^{\frac{1}{2}} = 5{\cdot}31 \times 10^5$ cm$^{-\frac{1}{2}}$. Figure 6 shows the results give a linear graph through the origin with a slope of $5{\cdot}53 \times 10^5$ cm$^{-\frac{1}{2}}$. Thus our measurements have confirmed that the collisionless skin depth is independent of frequency, is proportional to $n^{-\frac{1}{2}}$ and the constant of proportionality is correct within experimental error.

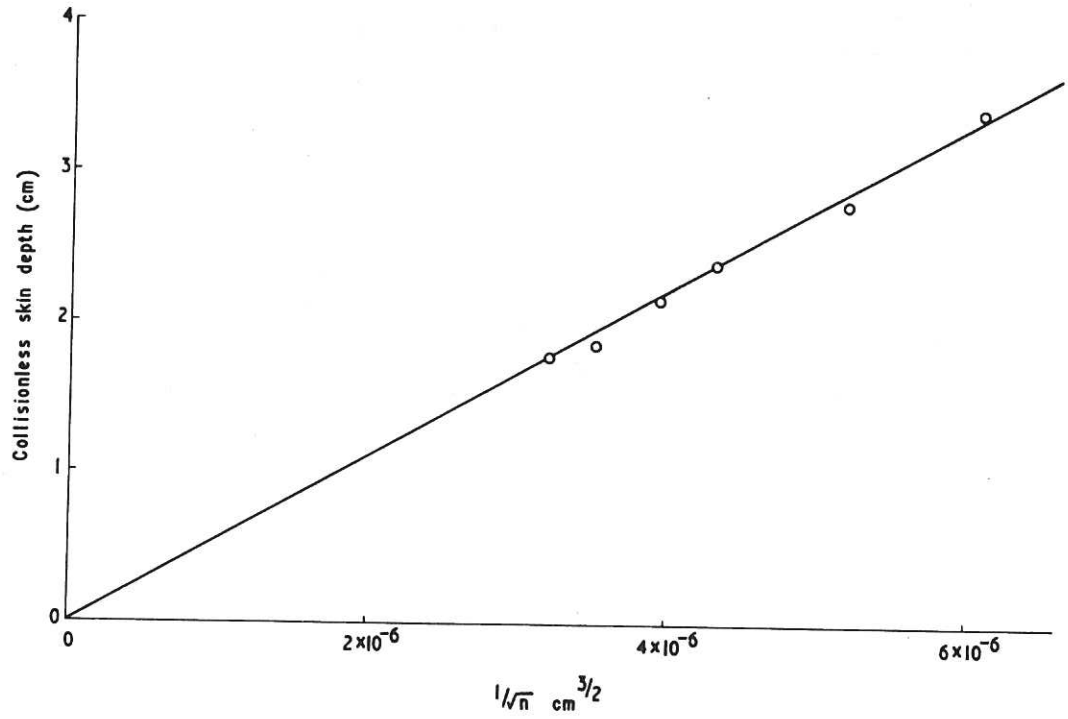

Fig. 6 (CLM-P 204)
Collisionless skin depth as a function of density

The measurements of electron density in the 13·6 amp arc were compared to the value found at a frequency much higher than the plasma frequency using an 8 mm micro-wave interferometer. The method was to measure the micro-wave phase change when the plasma was started. The phase change was only about 12^{o} and it was found that a spurious signal of at least this magnitude was caused by multiple reflections between the tube walls. The influence of these reflections on the result was reduced by plotting the observed signal as a function of wavelength. Since the signal due to multiple reflections depends on the number of wave-lengths between the reflecting surfaces whereas the direct signal is to first order independent of wavelength, the observed signal passes through maxima and minima as the wavelength is changed and the signal corresponding to the correct phase is the mean value. However, because of this correction and because the magnetic probe had to be removed to allow the microwaves to propagate across the tube diameter, the method was not as precise as, or exactly comparable to, the wave attenuation and Langmuir probe measurements. The final result gave an average electron density of $9{\cdot}2 \times 10^{10}$ cm^{-3} ± 20% compared to $8{\cdot}4 \times 10^{10}$cm^{-3} given by the wave attenuation measurement, and $8{\cdot}1 \times 10^{10}$cm^{-3} given by the Langmuir probe measurement. The agreement is satisfactory considering the uncertainties involved in the microwave measurement.

Table V also shows that the collision frequency calculated from the attenuation at high frequency is in agreement with the collision frequency calculated from Langmuir probe measurements using the d.c. potential drop. The collision frequency does not vary with electron density showing that electron-neutral, rather than electron-ion collisions are involved. This is to be expected since the electron-ion

collision frequency is negligible compared to the measured collision frequencies (the electron-ion collision frequency calculated from Spitzer's[14] resistivity formula including electron-electron encounters and taking an ion charge of unity varies from 0·018 MHz for the 4·6 amp arc to 0·065 MHz for the 16·2 amp arc).

By using the density of neutral atoms measured by the ion gauge, we can express the collision frequency in terms of the collision cross section (σ) times the electron velocity (v) averaged over the electron velocity distribution. The mean collision frequency from the Langmuir probe measurements was 1·20 MHz giving $\langle\sigma v\rangle = 7{\cdot}53 \times 10^{-7}$ cm sec^{-1}, and the mean collision frequency from the dispersion measurements was 1·08 MHz giving $\langle\sigma v\rangle = 6{\cdot}78 \times 10^{-7}$ cm sec^{-1}. These results are compared in Figure 7 to values computed from the measurements of Brode[15] giving the total probability of elastic

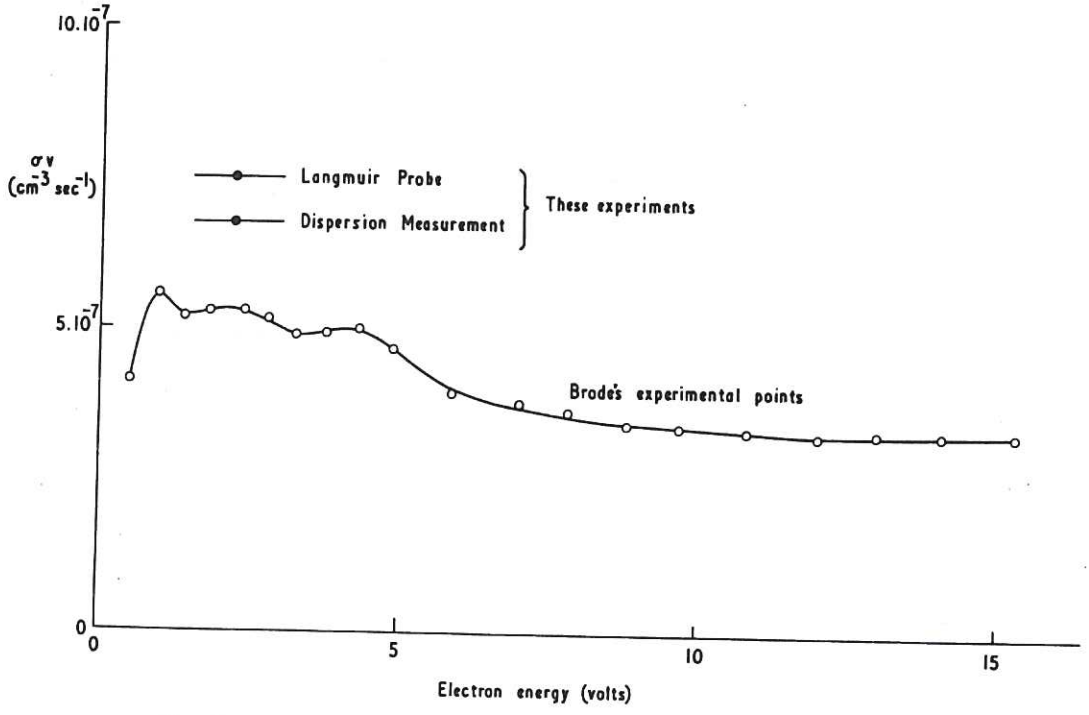

Fig. 7
(CLM-P 204)
Collision cross section times electron velocity as a function of electron energy from Brode's results compared to these experiments

and inelastic scattering of a beam of monoenergetic electrons through mercury vapour. It can be seen that Brode's results are around 25% less than these measurements. It is possible that, since the mean free paths ($= v/n_0 \sigma v \sim 11{\cdot}7$ cm for $\sigma v = 7{\cdot}53 \times 10^{-7}$ cm^3 sec^{-1} T = 2·2 eV) are greater than the tube radius, this may to some extent be connected with reflections at the sheath.

6. DISCUSSION

Necessary conditions for thermal effects to be appreciable in plane geometry are that both the electron mean free path and the radial distance moved by the electron during the time $1/\omega$ must exceed the skin depth. Figure 8 (calculated assuming a component of electron velocity parallel to the wave propagation direction of $1/\sqrt{3}$ times the thermal velocity) shows that these conditions are satisfied over

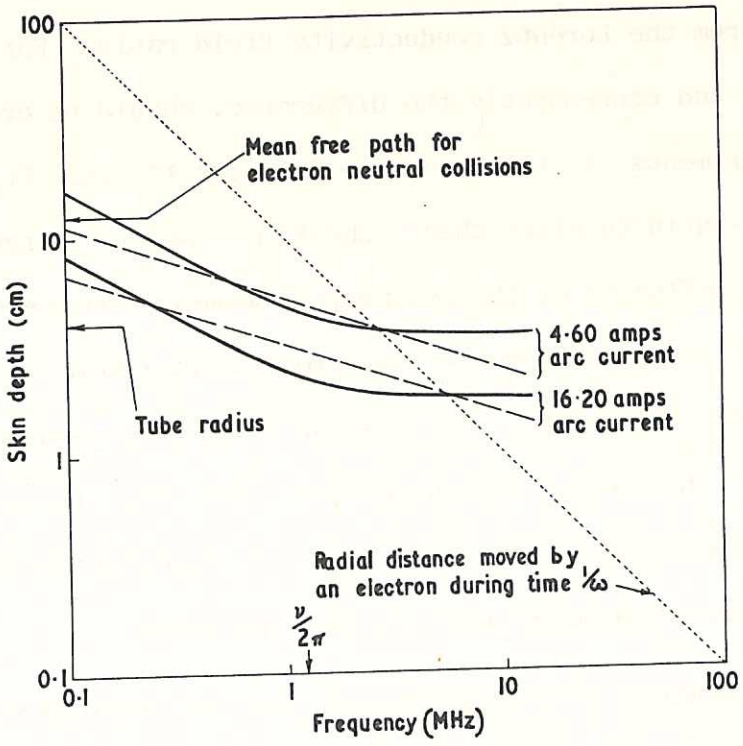

(CLM-P 204)

Fig. 8
Theoretical skin depth for these experiments assuming plane geometry compared to the electron mean free path and the radial distance moved by electrons during a time $1/\omega$ (continuous curve: complex conductivity skin depth: dashed curve: anomalous skin depth)

most of the frequency range. The anomalous skin depth, defined by Weibel as $2/\frac{d}{dx}(\log EE^*)$ at $x = 0$, is also shown since it is often compared with experiments although it should be remembered that it is not simply related to the field inside the plasma because the attenuation is not exponential.

Weibel's calculations using semi-infinite plane geometry and an electron reflecting plasma surface permit a more quantitative condition for appreciable thermal effects in terms of a parameter $\lambda = \frac{v^2}{\delta^2\omega^2}(1 + (\nu/\omega)^2)^{\frac{3}{2}}$. Although he stated that thermal effects deep in the plasma should become noticeable for $\lambda \gtrsim 0{\cdot}3$, interpolation of his results for $\omega = \nu$ show that a more stringent condition is required for the small field ratios measured in these experiments. For example, with $\lambda = 15$ and a field ratio of 2 (corresponding to the 16·2 amp arc current at $\omega = \nu$) Weibel's curves show that the field ratio differs by only 14% from the Lorentz conductivity field ratio. For lower arc currents, λ and consequently the difference, should be even less. In these experiments λ is between $\sim 0{\cdot}1$ and 15 (see Figure 9) so Weibel's semi-infinite plane theory should not predict large thermal effects. The influence of the cylindrical geometry on these predictions is not clear, although the experimental agreement with the Lorentz conductivity formula over most of the densities used show that this is small. The absolute value of the field ratio is, of course, not predicted by Weibel's semi-infinite plane calculations because of the cylindrical geometry used in the experiment.

The region where these experimental results deviated significantly from elementary theory based on the Lorentz conductivity was around a frequency of 7 MHz with the 16·2 amp arc current (see Figure 2).

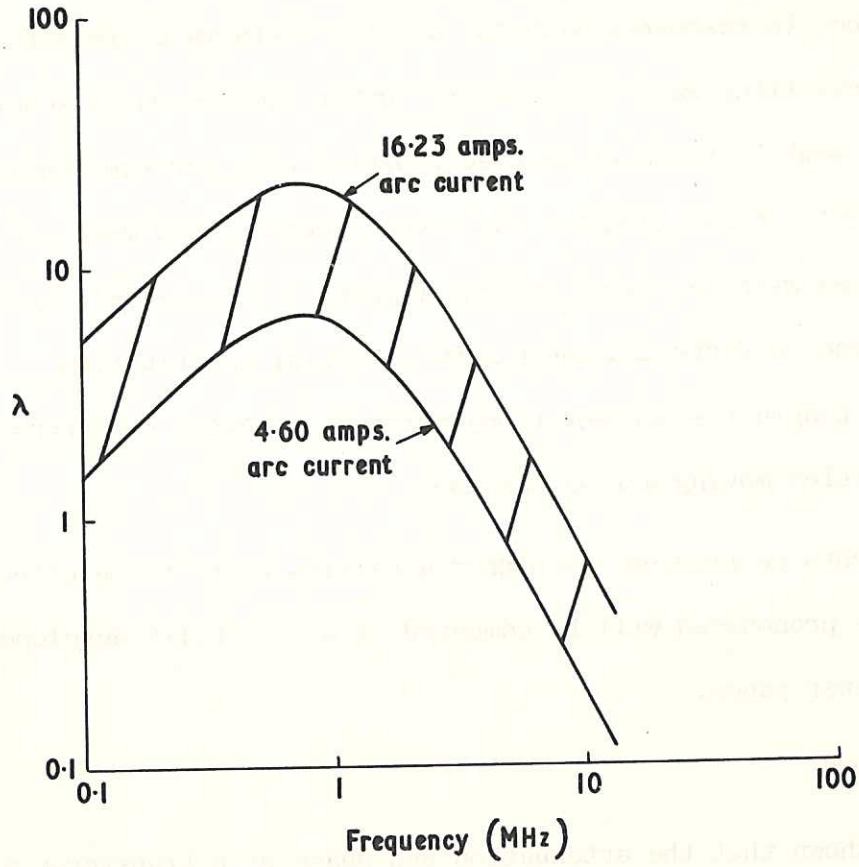

Fig. 9 (CLM-P 204)
Weibel's parameter λ calculated for these experiments

Then $\omega \sim 6\nu$, the magnetic field ratio is ~ 3, $\lambda \lesssim 3$ and the attenuation is enhanced above the elementary theory. Weibel's curves for $\omega = \nu$ predict enhanced attenuation for small $\lambda(\lesssim 1)$ and high field ratios ($\gtrsim 10$) and reduced attenuation for high λ and low field ratios leading to a variation in field ratio which is not monotonic. He ascribes this to electrons which carry momentum acquired near the surface to deeper layers where they are in or out of phase with the field. Unfortunately he does not present curves for higher frequencies. Nevertheless, we think the effect we observe for $\omega \sim 6\nu$ is physically similar to that predicted by Weibel modified, perhaps, by geometrical factors. These factors should make deviations from the elementary theory more pronounced because electrons can move from side to side

of the tube, successively sampling the strong surface field. They can thereby be in resonance with the applied field in a similar manner to a travelling wave accelerator. Other factors which should make Weibel's semi-infinite plane theory differ from our experiment are that in cylindrical geometry the wave electric field must vary with radius even with no plasma present (since $\nabla \times E = -\frac{\partial B}{\partial t}$), electron convergence effects and the plasma potential distribution (expressed by Langmuir's arc equation) which may prevent electrons of certain velocities moving across the tube.

Measurements carried out at higher densities where these effects should be more pronounced will be compared to a more fully developed theory in a later paper.

7. CONCLUSIONS

We have shown that the attenuation and phase of a transverse electromagnetic wave in a cylindrical plasma can be fitted to an elementary relation based on the Lorentz conductivity for an angular frequency range from $0{\cdot}1\nu$ to 10ν by a suitable choice of ν and electron density. For the electron density range $2{\cdot}7 \times 10^{10}$ cm^{-3} to $8{\cdot}1 \times 10^{10}$ cm^{-3} the electron density and collision frequency agree with measurements using a Langmuir probe at the tube wall. The influence of plasma non-uniformity, finite magnetic probe size and finite Debye length is small. When the wave frequency is much greater than the collision frequency, the attenuation of the wave is independent of frequency, the phase shift is zero and the results agree numerically with the collisionless skin depth. A greater attenuation than predicted by the elementary formula is observed in the collisionless regime with an electron density of $9{\cdot}8 \times 10^{10}$ cm^{-2}. It is postulated

that this is due to the finite electron thermal velocity.

8. ACKNOWLEDGEMENTS

The authors wish to thank Dr. K.V. Roberts for his support and encouragement. They are also grateful to J.A. Daniel for his large part in the experimental work, and to N.E. Couchmann and T.J. Martin for computations.

9. REFERENCES

1. PIPPARD, A.B., Proc. Roy. Soc. A191, 395 (1947)

2. REUTER, G.E.H. and SONDHEIMER, E.H., Proc. Roy. Soc. (London) A195, 336 (1948).

3. WEIBEL, E.S., Phys. Fluids, 10, 741 (1967).

4. CARRUTHERS, R. Appl. Sci. Research, 5, 135 (1955)

5. DEMIRKHANOV, R.A., LEONTEV, N.I., LOGVINOV, V.V. and UDOVICHENKO, Yu.K. Sov. Phys. Tech. Phys., 7, 921 (1963).

6. DEMIRKHANOV, R.A., KADYSH, I.Ya., and KHODYREV, Yu.S., Sov. Phys. JETP, 19, 791 (1964).

7. KOFOID, M.J. and DAWSON, J.M., Phys. Rev. Letters 17, 1086 (1966).

8. HOLT E.H., and HASKELL, R.E., "Foundations of Plasma Dynamics", Macmillan (1965)

9. ABRAMOWITZ, M. and STEGUN, I.A., "Handbook of Mathematic Functions" Dover Publications Inc., New York (1965).

10. TONKS, L. and LANGMUIR, I. Phys. Rev. 34, 876, (1929).

11. BOHM, D. "The Characteristics of Electric Discharges in Magnetic Fields". edited by A Guthrie and R.K. Wakerling, McGraw-Hill, New York (1949).

12. BOYD, R.L.F. Proc. Roy. Soc. A201, 22 (1950)

13. PARKER, J.V. California Institute of Technology Technical Report No.19, Nonr 220 (13), (1962).

14. SPITZER, L. Jr., "Physics of Fully Ionized Gases", No.3 Interscience Tracts on Physics and Astronomy, Interscience Publishers, John Wiley & Sons, Long, 139 (1962).

15. BRODE, R.B. Proc. Roy. Soc. A125, 134 (1929).

APPENDIX A

Correction for the finite magnetic probe size

To find the effect of finite magnetic probe dimensions we must solve equation (3) neglecting the displacement current term ω^2/c^2 in the plasma since $\omega \ll c/\delta$. This gives

$$B = C\, I_o\left(\frac{r}{\delta}\sqrt{\frac{\omega}{\omega+i\nu}}\right) + D\, K_o\left(\frac{r}{\delta}\sqrt{\frac{\omega}{\omega+i\nu}}\right) \quad \ldots (16)$$

where C and D are constants determined by the boundary condition at the plasma/probe interface (radius b).

We first note that the magnetic field in the probe is uniform since, from equation (3) with $\delta = \infty$, the ratio of magnetic field at a radius r to magnetic field on the axis is $J_o(r\omega/c)$ which is unity because for these experiments $r\omega \ll c$. Thus the boundary condition at the probe surface that the magnetic field is continuous gives

$$B_o = C\, I_o\left(\frac{b}{\delta}\sqrt{\frac{\omega}{\omega+i\nu}}\right) + D\, K_o\left(\frac{b}{\delta}\sqrt{\frac{\omega}{\omega+i\nu}}\right) \quad \ldots (17)$$

where B_o is now the uniform magnetic field within the probe on the axis of the plasma. The second boundary condition at the probe surface is that the electric field is continuous. Maxwell's electromagnetic equations give the electric field just inside the probe surface as $\frac{j\omega B_o}{c} \cdot \frac{b}{2}$ and the electric field just inside the plasma at $r = b$ as $-(\nu - i\omega)\frac{\delta^2}{c}\frac{\partial B}{\partial r}$ giving the boundary condition, using equation (16)

$$\frac{b}{2\delta}\sqrt{\frac{\omega}{\omega+i\nu}} \cdot B_o = C\, I_1\left(\frac{b}{\delta}\sqrt{\frac{\omega}{\omega+i\nu}}\right) - D\, K_1\left(\frac{b}{\delta}\sqrt{\frac{\omega}{\omega+i\nu}}\right) \ldots (18)$$

Also, as before, we use the boundary condition at the outer plasma surface that the magnetic field is continuous

$$B_a = C\, I_o\left(\frac{a}{\delta}\sqrt{\frac{\omega}{\omega+i\nu}}\right) + D\, K_o\left(\frac{a}{\delta}\sqrt{\frac{\omega}{\omega+i\nu}}\right) \qquad \ldots (19)$$

Eliminating the constants C and D between equations (17), (18) and (19) and rearranging by using Wronskian relations[9] between Bessel functions, we get

$$\frac{B_a}{B_o} = \frac{b^2}{2\delta^2}\left(\frac{\omega}{\omega+i\nu}\right)\left[I_o\left(\frac{a}{\delta}\sqrt{\frac{\omega}{\omega+i\nu}}\right)K_2\left(\frac{b}{\delta}\sqrt{\frac{\omega}{\omega+i\nu}}\right) - K_o\left(\frac{a}{\delta}\sqrt{\frac{\omega}{\omega+i\nu}}\right)I_2\left(\frac{b}{\delta}\sqrt{\frac{\omega}{\omega+i\nu}}\right)\right]$$

$\ldots$ (20)

To find the correction for finite probe dimensions required when equation (7) is used to get the plasma density when $\omega \gg \nu$ (the collisionless case), we expand equation (7)

$$\frac{B_a}{B_o} = I_o\left(\frac{a}{\delta}\cdot\frac{1}{1+\varepsilon}\right) = I_o\left(\frac{a}{\delta}\right) - \frac{a\varepsilon}{\delta}\, I_1\left(\frac{a}{\delta}\right)$$

where ε is the fractional correction to be added to the apparent ratio of the plasma radius to collisionless skin depth deduced from equation (7). Since a/δ is proportional to the square root of the plasma density, the correction required on the apparent density is

$$\frac{\Delta n}{n} = 2\varepsilon = 2\,\frac{I_o\left(\frac{a}{\delta}\right) - \frac{B_a}{B_o}}{\frac{a}{\delta}\cdot I_1\left(\frac{a}{\delta}\right)} \qquad \ldots (21)$$

or, using equation (20)

$$\frac{\Delta n}{n} = \frac{2}{\frac{a}{\delta}\, I_1\left(\frac{a}{\delta}\right)}\left[I_o\left(\frac{a}{\delta}\right) - \frac{b^2}{2\delta^2}\left(I_o\left(\frac{a}{\delta}\right)K_2\left(\frac{b}{\delta}\right) - K_o\left(\frac{a}{\delta}\right)I_2\left(\frac{b}{\delta}\right)\right)\right]$$

$\ldots$ (22)

Tables[9] show that, for the parameters used in these experiments ($a = 4{\cdot}05$ cm, $b = 0{\cdot}625$ cm, $\delta \sim 2$ cm),

$$I_0\left(\frac{a}{\delta}\right)\cdot K_2\left(\frac{b}{\delta}\right) \gg K_0\left(\frac{a}{\delta}\right)\cdot I_2\left(\frac{b}{\delta}\right)$$

and

$$\frac{1}{2}\left(\frac{b}{\delta}\right)^2 K_2\left(\frac{b}{\delta}\right) \doteq 1-\left(\frac{b}{2\delta}\right)^2$$

so equation (22) reduces to

$$\frac{\Delta n}{n} = \frac{a}{2\delta}\left(\frac{b}{a}\right)^2 \frac{I_0\left(\frac{a}{\delta}\right)}{I_1\left(\frac{a}{\delta}\right)} \qquad \ldots (23)$$

Since this is positive, the actual density is greater than the apparent density deduced using the simple formula (7).

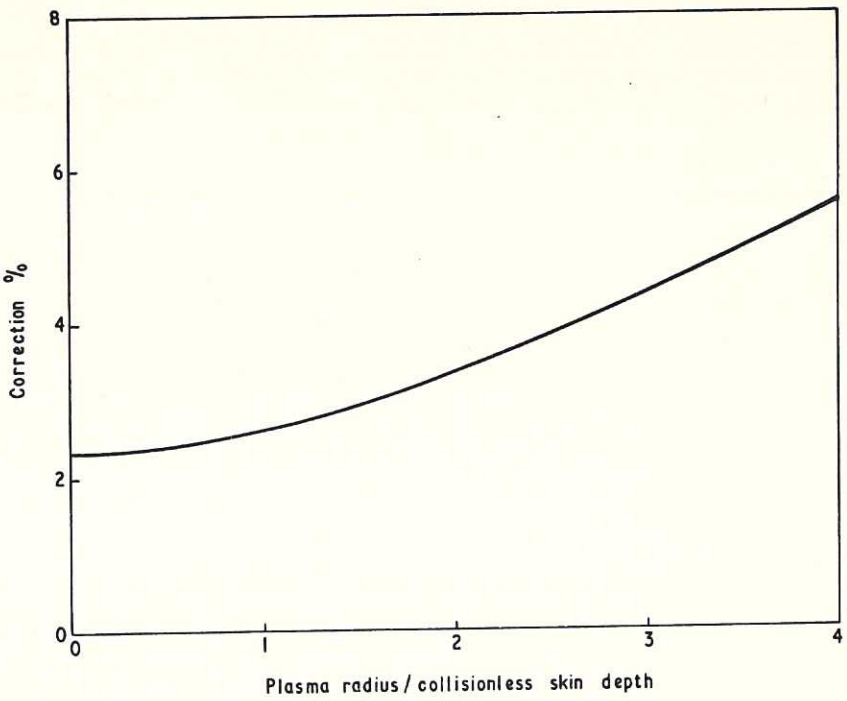

Fig. 10 (CLM-P 204)
Correction to density deduced from the collisionless equation (7) for finite magnetic probe dimensions (b/a = 0.154)

Figure 10 shows the correction $\frac{\Delta n}{n}$ plotted as a function of $\frac{a}{\delta}$ for the experimental ratio of probe radius to tube radius of 0·154.

For very small $\frac{a}{\delta}(\ll 2)$, equation (23) reduces to

$$\frac{\Delta n}{n} = \left(\frac{b}{a}\right)^2$$

or, if n^1 is the apparent density obtained using the simple equation (7),

$$\pi a^2 n^1 = \pi(a^2 - b^2)n$$

so equation (7) predicts the correct line density rather than the actual density.

APPENDIX B

Correction for plasma non-uniformity

The variation of electron density with radius may be derived by Langmuir's[10] series solution of equation 12. This may, to a good approximation, be expressed as

$$n = \hat{n}\left(1 - \Upsilon\left(\frac{r}{a}\right)^2\right)$$

where $\Upsilon = 0{\cdot}6$, giving the volume average density

$$\bar{n} = \frac{1}{\pi a^2}\int_0^a 2\pi r\, n\, dr = \hat{n}\left(1 - \frac{\Upsilon}{2}\right)$$

and

$$n = \bar{n}\left(\frac{1 - \Upsilon\left(\frac{r}{a}\right)^2}{1 - \frac{\Upsilon}{2}}\right) \qquad \ldots (25)$$

We will now derive the wave magnetic field using this variation of density as a function of radius. In order to avoid density gradients in the final equation, we will first find the dispersion equation for the wave electric field, then use Maxwell's equation $\nabla \times \underline{E} = j\omega B/c$ to give the dispersion equation for the wave magnetic field. Neglecting displacement currents, equations (2), (25) and Maxwell's equations give

$$\frac{1}{E}\frac{\partial}{\partial r}\left[\frac{1}{r}\frac{\partial}{\partial r}(Er)\right] = \frac{1}{\delta^2}\left(\frac{1 - \Upsilon\left(\frac{r}{a}\right)^2}{1 - \frac{\Upsilon}{2}}\right)\cdot\frac{\omega}{\omega + i\nu}$$

where $\bar{\delta} = \sqrt{mc^2/4\pi\bar{n}e^2}$, the collisionless skin depth using the volume average density. The substitutions

$$Za = Er\ ,\ \eta = \frac{a}{4\delta}\sqrt{\frac{\omega}{(\omega + i\nu)\,\Upsilon(1 - \Upsilon/2)}} \quad \text{and} \quad \rho = 2\Upsilon\eta\left(\frac{r}{a}\right)^2$$

reduce the equation to the standard form

$$\frac{\delta^2 Z}{\delta \rho^2} + Z\left(1 - \frac{2\eta}{\rho}\right) = 0 \ .$$

The solution which is zero at the axis is

$$Z = \frac{Er}{a} = C_1 \cdot F_o(\eta\ ,\ \rho)$$

where $F_o(\eta\ ,\ \rho)$ is a Coulomb Wave Function[9] and C_1 is a constant. Converting this to the dispersion equation for the wave magnetic field by using Maxwell's equation $\frac{1}{r}\frac{\partial}{\partial r}(Er) = \frac{i\omega B}{c}$ we get

$$B = \frac{4\Upsilon\eta C_1 c}{i\omega a} F_o^1\ (\eta\ ,\ \rho)$$

Applying the boundary conditions that $B = B_a$ at $r = a$ and $B = B_o$ at $r = 0$

$$\frac{B_a}{B_o} = \frac{F_o^1(\eta\ ,\ 2\Upsilon\eta)}{F_o^1(\eta\ ,\ o)} = \sum_{N=1}^{\infty} N\ G_N(2\Upsilon\eta)^{N-1} \qquad \ldots\ (26)$$

where

$$G_1 = 1\ ,G_2 = \eta \quad \text{and} \quad G_N\ N(N-1) = 2\eta\ G_{N-1} - G_{N-2} \ \ldots\ (27)$$

We may now find the correction in the apparent density required when we use the simple equation (4) rather than equation (26), knowing the value of Υ. Taking as an example the collisionless extreme when $\omega \gg \nu$ and the attenuation is a maximum, the correction is, from equations (21) and (26),

$$\frac{\Delta n}{n} = -2\ \frac{\left[\sum_{N=1}^{\infty} N\ G_N(2\Upsilon\eta)^{N-1} - I_o\left(\frac{a}{\delta}\right)\right]}{\frac{a}{\delta}\ I_1\left(\frac{a}{\delta}\right)}$$

This is negative, so the correction tends to cancel the correction required for the finite probe diameter. For $\Upsilon = 0{\cdot}6$ this becomes

$$\frac{\Delta n}{n} = - \frac{0{\cdot}468 \left(\frac{a}{\delta_{\parallel}}\right)^2 + 3{\cdot}07 \times 10^{-2} \left(\frac{a}{\delta_{\parallel}}\right)^4 + 8{\cdot}33 \times 10^{-4} \left(\frac{a}{\delta_{\parallel}}\right)^6 + \cdots}{1 + 0{\cdot}125 \left(\frac{a}{\delta_{\parallel}}\right)^2 + 5{\cdot}22 \times 10^{-3} \left(\frac{a}{\delta_{\parallel}}\right)^4 + 1{\cdot}086 \times 10^{-4} \left(\frac{a}{\delta_{\parallel}}\right)^6 + \cdots} \%$$

This is plotted in Figure 11

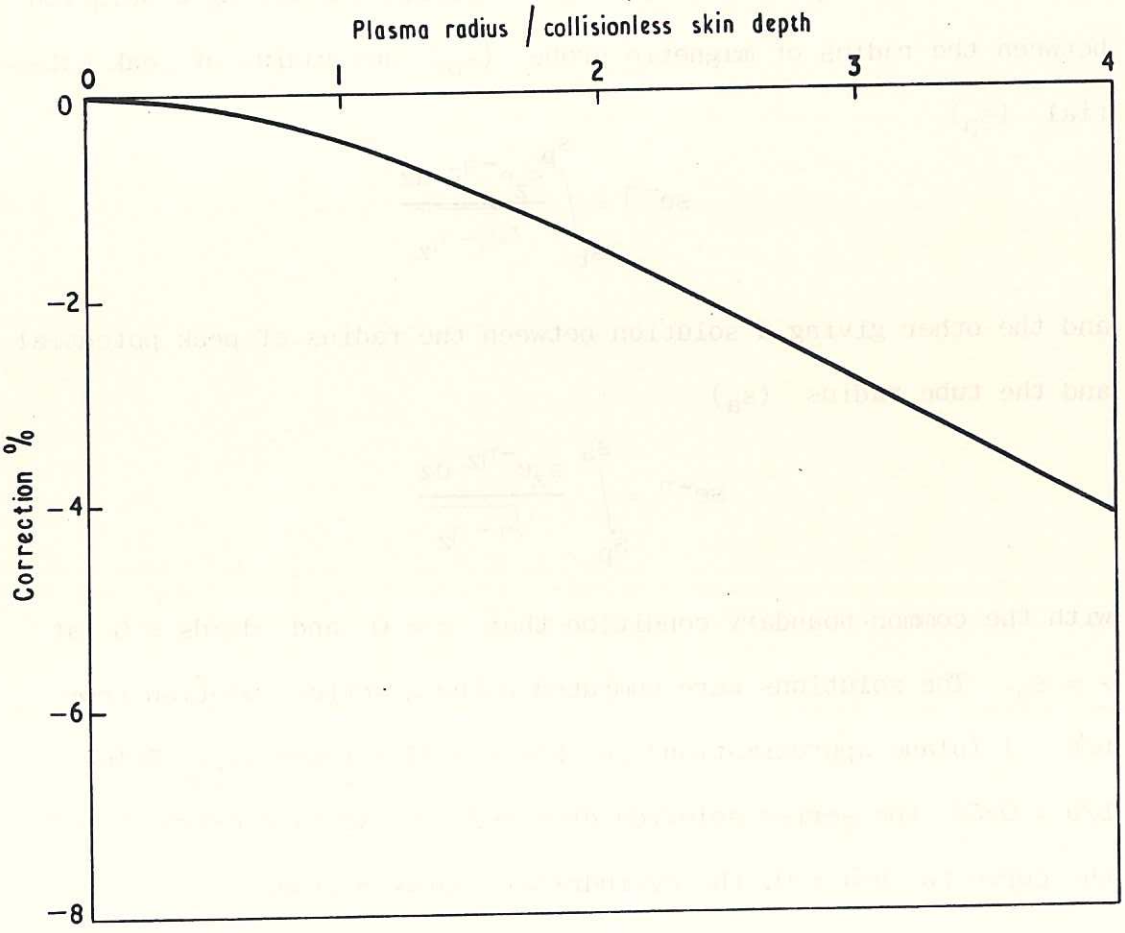

Fig. 11 (CLM-P 204)
Correction to the density deduced from the collisionless equation (7) for density gradients using $\gamma = 0.6$

APPENDIX C

Correction to the Langmuir probe equation for the presence of the magnetic probe

A sheath is formed at the magnetic probe surface as well as at the discharge tube wall. Consequently, there is a peak in the plasma potential between the probe and discharge tube wall. To calculate the correction on the average density deduced using the simple equation (14), we divide equation (12) into two parts, one giving a solution between the radius of magnetic probe (s_b) and radius of peak potential (s_p)

$$se^{-\eta} = \int_{s_b}^{s_p} \frac{s_z e^{-\eta_z}\, dz}{\sqrt{\eta - \eta_z}}$$

and the other giving a solution between the radius of peak potential and the tube radius (s_a)

$$se^{-\eta} = \int_{s_p}^{s_a} \frac{s_z e^{-\eta_z}\, dz}{\sqrt{\eta - \eta_z}}$$

with the common boundary condition that $\eta = 0$ and $d\eta/ds = 0$ at $s = s_p$. The solutions were computed using a series solution from $b/a = 1$ (plane approximation) to $b/a = 0{\cdot}35$ (Figure 12). Below $b/a = 0{\cdot}35$ the series solution diverged, and we have extrapolated the curve to $b/a = 0$, the cylindrical approximation.

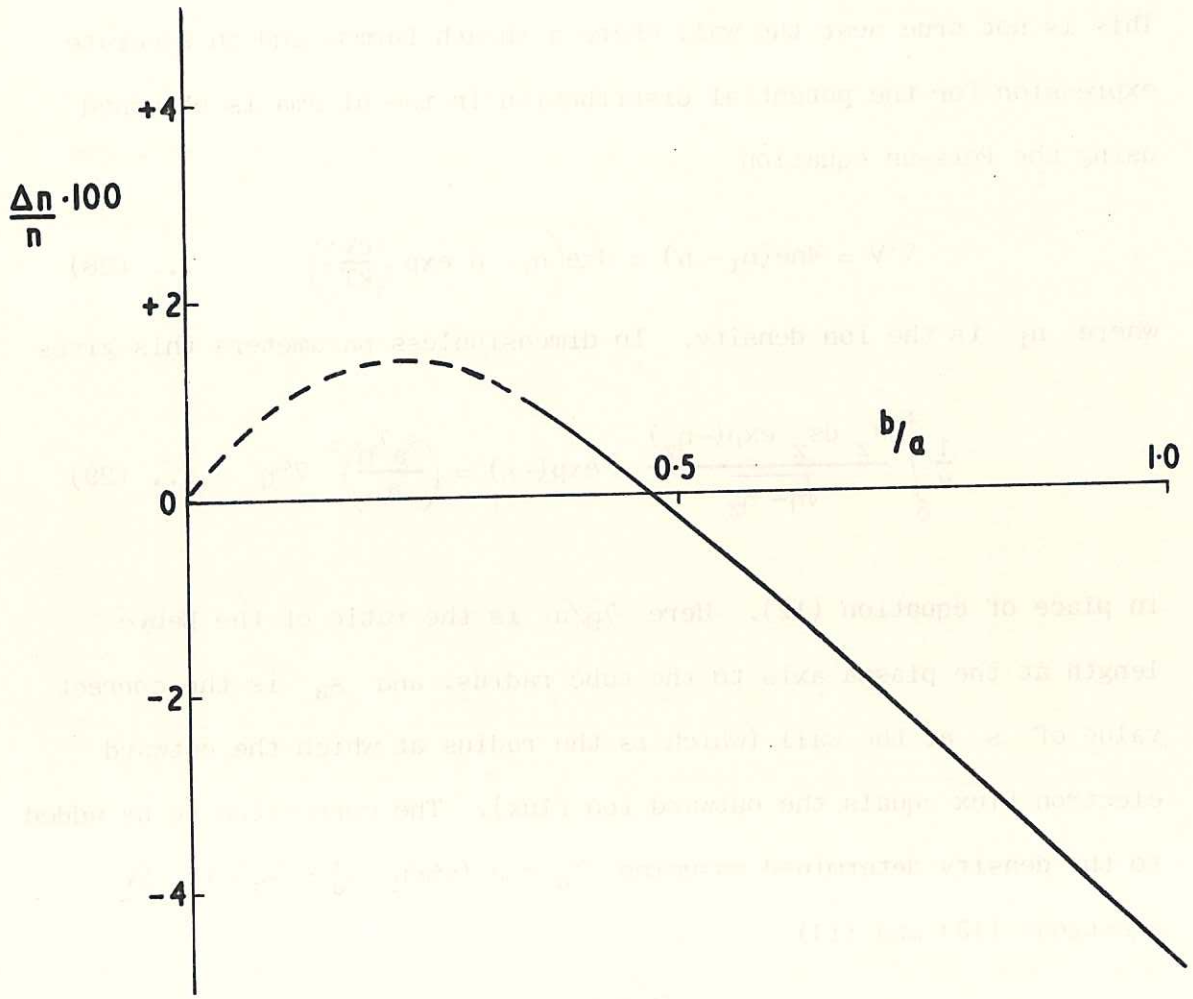

Fig. 12 (CLM - P 204)
Correction to the density deduced from Langmuir's probe for the presence of the magnetic probe

APPENDIX D

Correction to the Langmuir probe equation for the finite Debye length

In deriving the probe equation (14) we assumed that at all points across the radius, the ion density was the same as the electron density. This is not true near the wall where a sheath forms, and an accurate expression for the potential distribution in the plasma is obtained using the Poisson equation

$$\nabla^2 V = 4\pi e(n_i - n) = 4\pi e\left(n_i - \hat{n}\exp\left(\frac{eV}{kT}\right)\right) \qquad \ldots (28)$$

where n_i is the ion density. In dimensionless parameters this gives

$$\frac{1}{s}\int_0^s \frac{s_z\, ds_z \exp(-\eta_z)}{\sqrt{\eta - \eta_z}} - \exp(-\eta) = \left(\frac{s_a \lambda_D}{a}\right)^2 \nabla^2\eta \qquad \ldots (29)$$

in place of equation (12). Here λ_D/a is the ratio of the Debye length at the plasma axis to the tube radius, and s_a is the correct value of s at the wall (which is the radius at which the outward electron flux equals the outward ion flux). The correction to be added to the density determined assuming $\lambda_D \ll a$ (when $s_a^1 = s_a$) is, by equations (13) and (14)

$$\frac{\Delta n}{n} = \frac{s_a^1 - s_a}{s_a} \cdot 100\%$$

Parker[13] has solved numerically equation (29) in cylindrical geometry, and using his value of s_a we have computed the correction as a function of λ_D/a. The results are shown in Figure 13.

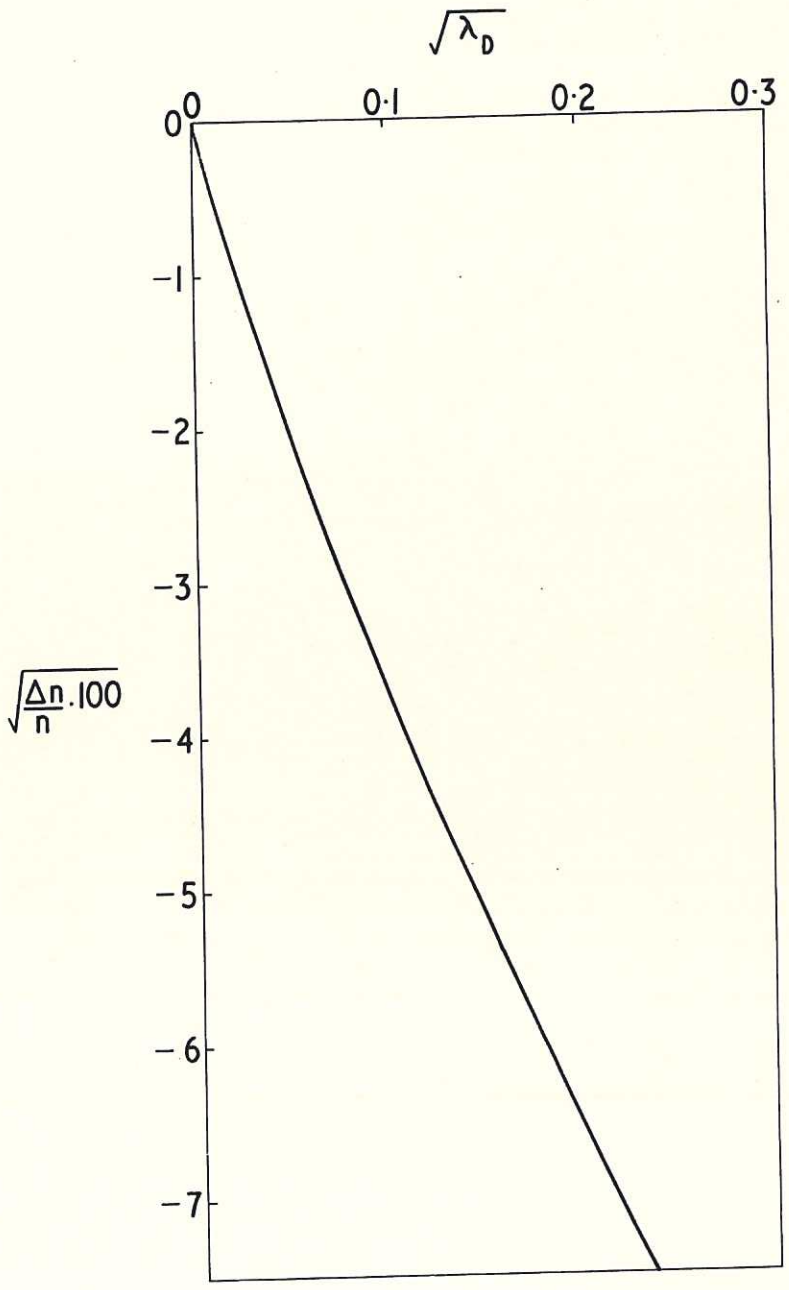

(CLM-P 204)

Fig. 13
Correction to the density deduced from Langmuir's probe for the finite Debye length

For small λ_D/a ($< \sim 3 \times 10^{-3}$), the curve gives approximately

$$\frac{\Delta n}{n} = - 1{\cdot}6 \times 10^{3} \frac{\lambda_D}{a} \%$$

SYMBOLS

A	ratio of the amplitude of the magnetic field at the plasma surface to the amplitude of the magnetic field at the plasma axis.
a	plasma radius
B	wave magnetic field at a radius r
B_a	wave magnetic field at the plasma surface, r = a
B_o	wave magnetic field at the plasma axis, r = 0
b	magnetic probe radius
C	arbitrary constant
C_1	arbitrary constant
c	velocity of light
D	arbitrary constant
E	electric field at a radius r
e	electron charge
F_o	Coulomb wave function of zero order
F_o^1	$\partial F_o / \partial \rho$
G_N	defined by equation 26
I	ion current density to the discharge tube wall
I_o	modified Bessel Function of zero order and first kind
I_1	modified Bessel Function of first order and first kind
I_2	modified Bessel Function of second order and first kind
i	$\sqrt{-1}$
J	current density
J_o	Bessel Function of zero order and first kind
K_o	modified Bessel Function of zero order and second kind
K_1	modified Bessel Function of first order and second kind
K_2	modified Bessel Function of second order and second kind
k	Boltzmann's constant
ℓ	distance between Langmuir probes

M	ion mass
m	electron mass
n	electron density at a radius r
$\bar{n}$	average electron density defined by equation 9
$\hat{n}$	peak electron density
n^1	apparent electron density neglecting effect of finite probe radius
n_o	neutral atom density
n_i	ion density at a radius r
p	radius of peak electric field
r	radius
s	dimensionless radius defined by equation 13.
s_a	s at r = a
s_b	s at r = b
s_p	s at r = p
s_a^1	S at r = a assuming $\lambda \ll a$
s_z	S at r = z
T	electron temperature
t	time
v	electron velocity
V	plasma potential at radius r
Z	dimensionless electric field by $Za = Er$
z	a radius less than r
β	$\frac{1}{4}(a/\delta)^2 \frac{\omega^2}{\omega^2 + \nu^2}$
γ	constant governing the variation of density with radius
δ	collisionless skin depth at radius r
$\bar{\delta}$	collisionless skin depth corresponding to the average density, $\bar{n}$
δ_c	collisional skin depth at radius r

ε correction to a/δ for finite magnetic probe diameter

η dimensionless plasma potential, $-\frac{eV}{kT}$

η $\frac{a}{4\bar{\delta}} \left(\frac{\omega}{(\omega + i\nu)\Upsilon(1 - \Upsilon/2)} \right)^{\frac{1}{2}}$

η_z dimensionless plasma potential at radius z

θ phase angle

λ Weibel's parameter

λ_D Debye length at peak density

ρ $2\,\Upsilon\eta\ (r/a)^2$

σ conductivity

σ electron collision cross section for momentum transfer

φ potential drop between Langmuir probes

ν collision rate for electron momentum transfer

ω wave angular frequency

ber_o real Kelvin function of zero order and first kind

bei_o imaginary Kelvin function of zero order and first kind